FULL PAPER

In Situ Studies of Ion Transport in Microporous Supercapacitor Electrodes at Ultralow Temperatures

Yair Korenblit, Adam Kajdos, William C. West, Marshall C. Smart, Erik J. Brandon, Alexander Kvit, Jacek Jagiello, and Gleb Yushin*

The ability to quickly store and deliver a significant amount of electrical energy at ultralow temperatures is critical for the energy-efficient operation of high altitude aircraft and spacecraft, exploration of natural resources in polar regions and extreme altitudes, and astronomical observatories exposed to ultralow temperatures. Commercial high-power electrochemical capacitors fail to operate at temperatures below –40 °C. According to conventional wisdom, mesoporous electrochemical capacitor electrodes with pores large enough to accommodate fully solvated ions are needed for sufficiently rapid ion transport at lower temperatures. It is demonstrated that strictly microporous carbon electrodes with much higher volumetric capacitance can be efficiently used at temperatures as low as –70 °C. The critical parameters, with respect to electrolyte properties and electrode porosity and microstructure, needed for achieving both rapid ion transport and efficient ion electroadsorption in porous carbons are discussed. As an example, the fabrication of an electrochemical capacitor with an outstanding performance at temperatures as low as –60 and –70 °C is demonstrated. At such low temperatures the capacitance of the synthesized electrodes is up to 123 F g^{-1} ($\approx$76 F cm^{-3}), which is 50–100% higher than that of the most common commercial electrochemical capacitor electrode at room temperature. At –60 °C selected cells based on $\approx$0.2 mm electrodes exhibited characteristic charge–discharge time constants of less than 9 s, which is faster than the majority of commercial devices at room temperature. The achieved combination of high energy and power densities at such ultralow temperatures is unprecedented and extremely promising for the advancement of energy storage systems.

1. Introduction

The need to develop efficient, rechargeable, and high-power energy storage devices that can operate at temperatures significantly lower than those currently attainable stems from the growing industrial and scientific explorations of low-temperature regions,[1] astronomical observatories necessitating operations in polar regions and extreme altitudes,[2] severe fluctuations in global temperatures,[3] the development of electrical aerial vehicles, and the growing applications of energy storage devices in space and high altitude aircraft.[2,4] In cold and polar regions, as well as at extreme altitudes, high-power energy storage devices are needed for use in wind-turbine pitch control, in optimizing intermittent solar power utilization, as power sources for communication devices, sensors and other electronic devices, for cold-cranking gasoline and diesel engines, and for regenerative braking and acceleration in hybrid electric vehicles (HEVs). In unmanned and manned aerial vehicles high-power energy storage devices are needed for manipulating wing pitch and other peak power applications described in the US Air Force's initiative in electrifying aerial vehicles.[5]

Both the severely reduced electrolyte conductivity and dramatically hampered solid state diffusion of Li ions through the solid electrolyte interphase (SEI) and the active electrode particles used in the construction of high-power rechargeable Li-ion batteries currently limit commercial products to a minimum operational temperature of –20 °C.[6] Some of these limitations can be circumvented by using electrochemical double layer capacitors (EDLCs), often termed supercapacitors. Such alternative high-power electrochemical energy storage devices do not require solid state diffusion and permit a stable operation with a much wider variety of electrolyte salts and solvents.[7] Thus, they are of particular interest for further development and use at ultralow temperatures.[8]

Supercapacitors have seen a major increase in attention in the past few years.[7,9] The interest in these devices takes root in their ability to reach energy density levels that are orders of magnitude higher than solid-state capacitors while providing power densities much higher than any available battery.[7] The

Y. Korenblit, A. Kajdos, Prof. G. Yushin
School of Materials Science and Engineering
Georgia Institute of Technology
Atlanta, GA 30332-0245, USA
E-mail: yushin@gatech.edu
Dr. W. C. West, Dr. M. C. Smart, Dr. E. J. Brandon
Jet Propulsion Laboratory
California Institute of Technology
Pasadena, CA 91109, USA
Prof. A. Kvit
Materials Science Center and Materials Science Department
University of Wisconsin–Madison
Madison, WI 53706, USA
Dr. J. Jagiello
Micromeritics Instrument Corp
Norcross, GA 30093, USA
Dr. G. Yushin
Streamline Nanotechnologies
Inc., Atlanta, GA 30332-0100, USA

FULL PAPER

current applications of these important devices include electric vehicles (EVs) and HEVs, energy efficient industrial equipment, improving power quality and other applications requiring long cycle life, moderately high energy density and charging within seconds or less.[7a]

Most commercial EDLCs are based on activated carbon electrodes separated by an ion-permeable membrane and immersed in a liquid electrolyte. The primary mechanism for energy storage of EDLCs is based on the electrostatic adsorption of electrolyte ions on the large specific surface area and electrically conductive electrodes. For a given electrolyte, the energy storage characteristics of EDLCs are largely determined by the ability of their electrodes to adsorb a large quantity of ions under an applied potential.[10] Their power characteristics, in turn, are governed by the rate at which ions from an electrolyte solution can be delivered to and adsorbed on the available electrode surface area during charging.[10]

Improving power density of EDLCs can be achieved by improving the rate of ion transport within the porous carbon electrodes,[9e,9k,11] minimizing the ion diffusion distance[12] or by utilizing both approaches.[13] However, the overall electrochemical characteristics of the system should be carefully considered when approaching the synthesis routes of the various components. For example, by forming large interconnected mesopores and minimizing, or altogether eliminating the micropores within the electrode materials, the average coefficient of ion diffusion within carbon can be enhanced, but at the expense of a greatly reduced volumetric capacitance and an increased amount of electrolyte needed to fill the enlarged electrode pore volume. With respect to the entire electrochemical cell, as the relative weight of electrolyte becomes higher than the weight of carbon, both volumetric and gravimetric energy density will be reduced. Therefore, while electrodes produced from highly porous electrodes such as carbon onions,[9e,13a] carbon nanotubes,[9e,13c] and graphene[11c,13b] offer high power density to EDLCs, their excessive pore volume inevitably reduces the energy density of the fabricated devices. Similarly, the reduction of the electrode thickness from 200-300 μm[9k,11a,14] to a few micrometers or below[13a,13b] greatly reduces the average ion path length and thus dramatically decreases the characteristic charging time. However, this reduction leads to a major increase in the relative weight and volume of the inactive device components (such as metal foil current collectors and separator membrane) and thus will significantly reduce both the gravimetric and volumetric energy density of the fabricated devices.

Commercial EDLCs with activated carbon electrodes and electrolyte composed of 1 M solution of tetraethylammonium tetrafluoroborate (TEA-BF$_4$) salt in acetonitrile (AN) solutions fail to operate at temperatures below –40 °C.[8b] In our prior studies we investigated electrodes utilizing commercial mesoporous activated carbon with an average pore size of 3.6 nm in an electrolyte consisting of TEA-BF$_4$ salt in AN mixed with 25 vol% of low freezing point co-solvents, such as methyl acetate (MA), methyl formate (MF), and 1,3-dioxolane (DIOX) in order to extend the low temperature limit of EDLC operation. The relatively large pore size of activated carbons was selected in order to allow fully solvated ions to move within the carbon pores at low temperatures, where thermal energy could be too low for distortion or partial removal of ion solvation shells. We

demonstrated stable operation at temperatures as low as –70 °C.[8] However, at the lowest temperatures a significant decrease in the maximum operating frequency was commonly observed. Additionally, even when the cells were discharged slowly they could not demonstrate a specific electrode capacitance above ≈40 F g^{-1} (≈16 F cm^{-3}), which is only 50% of commercial EDLCs at room temperature (≈80 F g^{-1}). The low volumetric capacitance is explained largely by the large carbon pore size, which was shown to demonstrate significantly inferior capacitance than small micropores.[15]

Here we demonstrate that strictly microporous carbons allow rapid ion transport and improved capacitive storage characteristics at temperatures as low as –70 °C.

2. Results and Discussion

Formation of uniformly sized micropores in activated carbons is challenging. Microporous carbide-derived carbons[15a,16] exhibit narrow pore size distribution but suffer from tortuous pore shape, which affect the ion transport in micropores.[9l] In contrast, the use of sacrificial zeolite templates for porous carbon synthesis, initially proposed by Kyotani[17] and later adopted by several other groups (see e.g., ref. [9d,9f,9l]), allow formation of straight ordered and interconnected micropores. In our studies we thus selected the robust zeolite lattice as a template for microporous carbon synthesis. Microporous zeolite-templated carbons (ZTC) were prepared by the decomposition of acetylene (C$_2$H$_2$) precursor into a carbon coating on the internal surface of a zeolite NaY powder template. In contrast to most of the prior work, however, we performed carbon deposition at low pressures (<10 Torr) and relatively low temperature (700 °C) to achieve a high carbon coating uniformity. Two ZTC samples were additionally heat-treated at 800 °C and 900 °C for one hour in a dynamic vacuum (flowing Ar) environment. Removal of the zeolite NaY powder template was achieved via etching in hydrofluoric acid, followed by removal of the remaining impurities using sulfuric acid and a final powder filtration and wash with distilled water until achieving a neutral pH.

The retention of the zeolite shape by the ZTC particles was confirmed by scanning electron microscopy (SEM) and transmission electron microscopy (TEM) studies (**Figure 1**a–c). In contrast to our previous study in which low pressures were not employed,[9d] a highly uniform structure of ZTC has been attained (Figure 1b,c) with no macropores or thick multilayered graphitic regions visible by TEM. Our previously reported X-ray diffraction (XRD) studies revealed a higher degree of pore alignment in ZTC samples heat-treated prior to zeolite etching.[11a] This heat-treatment procedure not only reduced the defects in carbon and assisted in the retention of the zeolite pore shape,[11a] but also increased the specific surface area and the total pore volume of ZTC as revealed by our investigation utilizing nitrogen sorption measurements (**Figure 2**a,b). The isotherms show virtually no hysteresis, indicative of the absence of the capillary condensation phenomena and thus the lack of significant mesopore content.[19] Density functional theory (DFT) calculations confirmed that all three ZTC samples consist mostly of micropores and exhibit moderately high specific surface area (SSA, Figure 2,b) and pore volume (Figure 2b).
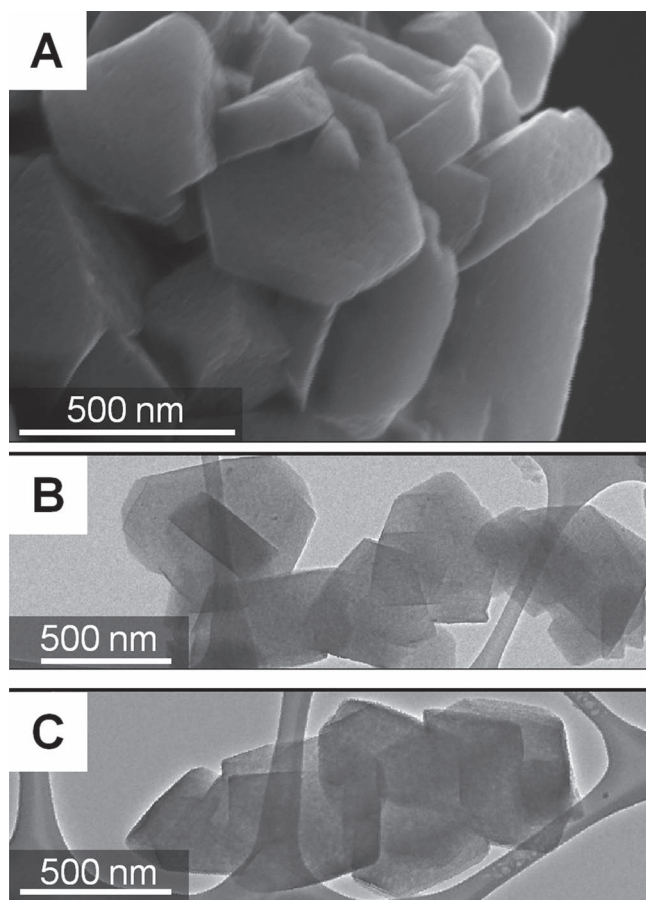
Materials
Views
www.MaterialsViews.com

ADVANCED
FUNCTIONAL
MATERIALS
www.afm-journal.de

Figure 1. Microstructure of synthesized zeolite NaY–templated carbon powder: a) SEM and b,c) TEM images of carbon particles showing replication of zeolite shapes and high uniformity of carbon particles.

Figure 2. Porosity characterization of synthesized zeolite NaY–templated carbon powder: a) N_2 sorption isotherms recorded at 77 K and b) pore size distribution in carbon calculated using slit-pore non-local DFT model. The SSAs in (a) were calculated according to the Brunauer–Emmett–Teller (BET) equation.

Electrochemical characterization of ion transport and electroadsorption in microporous carbons were performed in both standard electrolyte (TEA-BF$_4$ in AN) and in an electrolyte consisting of a solution of spiro-(1,1')-bipyrrolidinium tetrafluoroborate (SBP-BF$_4$) salt in a 1:1 (vol%) mixture of AN and MF. We chose MF as a co-solvent for the present study due to its low melting point (–100 °C), moderate dielectric constant ($\varepsilon = 8.5$) and low viscosity (0.319 cP at 29 °C). Our interest in studying a system consisting of SBP-BF$_4$ salt rather than the common TEA-BF$_4$ was motivated by SBP-BF$_4$'s higher ionic conductivity at low temperatures, observed when used with pure propylene carbonate solvent in an EDLC configuration.[18] Finally, keeping the salt concentration at least as low as 0.5 M allowed us to avoid salt precipitation at low temperatures, previously observed in EDLCs with TEA-BF$_4$ salt below –40 °C.

The ionic conductivity of the standard electrolyte is higher than that of SBP-BF$_4$ in 1:1 AN:MF from room temperature down to approximately –55 °C, where the standard electrolyte freezes (**Figure 3**). As expected, increasing the salt concentration supports a higher conductivity. However, if the electrolyte concentration is too high, the equivalent series resistance (ESR) of EDLCs steadily increases over time at such low temperatures due to salt precipitation on the carbon electrode surface.[8]
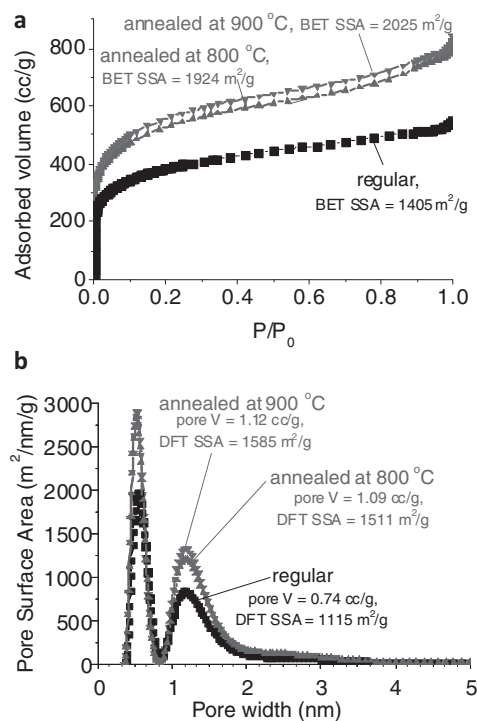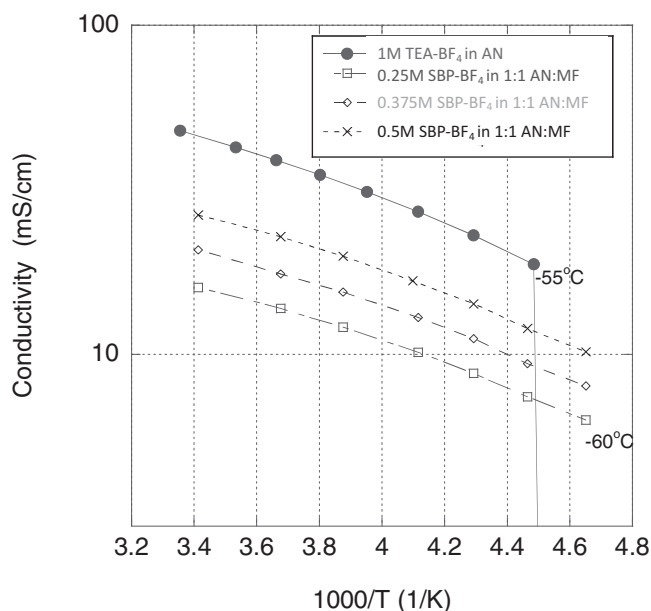

Figure 3 Conductivity of conventional (1 M solution of TEA-BF$_4$ salt in AN) and newly developed (0.25 M, 0.375 M, and 0.5 M solutions of SBP-BF$_4$ salt in 1:1 mixture of AN and MF) electrolytes as a function of temperature. The rapid drop in conductivity of a conventional electrolyte is visible at below –55 °C.
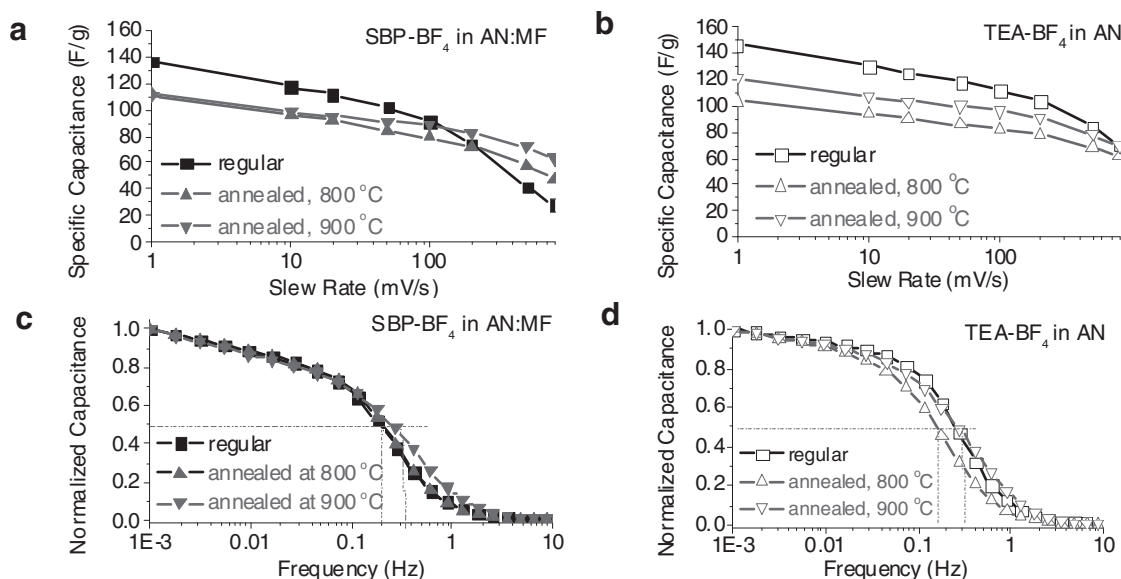
Figure 4. Room temperature performance of EDLCs in conventional (TEA-BF$_4$ in AN; hollow symbols) and newly developed (SBP-BF$_4$ in AN:MF = 1:1; solid symbols) electrolytes: a,b) specific capacitance calculated from the CV curves as a function of sweep rate; c,d) frequency response of capacitances. Zeolite-templated carbons synthesized at 700 °C (regular and annealed for one hour at 800 and 900 °C) were used in the EDLCs.

Cyclic voltammetry measurements at the sweep rate of 1 mV s^{-1} showed high specific capacitances for all ZTC samples when measured at room temperature (RT) in both electrolytes (**Figure 4**a,b). The most disordered sample[11a] (termed "regular" in the figures) consistently showed the highest capacitance (136–146 F g^{-1}; ≈84–90 F cm^{-3}) at 1 mV s^{-1} and the smallest capacitance retention at high current densities (Figure 4a,b). Prior studies revealed that defects and functional groups on the carbon surface may interact with both the ions and the solvent molecules in organic electrolytes, distorting the solvation shells and leading to the enhancement of specific capacitance normalized per unit area.[9e] This could be due to both the presence of a reversible pseudocapacitive behavior[9h,20] and the closer approach of the ions to the electrode surface, either by reduction of the solvation shell thickness or partial desolvation through distortion of the shell.[15a] A decreased charge separation distance is known to lead to higher capacitance, as observed in disordered microporous carbons.[15a]

The RT specific capacitance of carbons in both types of electrolyte was similar (within 10%) (Figure 4a,b). Some samples (e.g., a "regular" and annealed at 900 °C) showed marginally higher capacitance in the standard electrolyte while others (e.g., the one annealed at 800 °C) exhibited slightly higher capacitance in SBP-BF$_4$/AN:MF electrolyte. Such small variations are to be expected and rationalized by the complex electrode–electrolyte interactions affecting the specific capacitance. Parameters influencing the capacitance, include but are not limited to, the interplay between the carbon pore size and the size of the solvated and de-solvated ions,[15,21] local curvature of the carbon surface,[9k,15c,15d,22] interaction of the electrolyte with dopants,[9f] and functional groups[9g,9i] and defects on the carbon surface.[9e] Nonetheless, it appears that the higher conductivity of the standard electrolyte (Figure 3) leads to slightly better

ion transport properties and capacitance retention at higher sweep rates at RT (Figure 4a versus b). We also observed that the sample annealed at 900 °C possessed the most aligned pore structure (as revealed by our prior XRD measurements)[11a] and consistently showed the best capacitance retention, supporting our previous observations in aqueous electrolytes.[11a]

The RT frequency response of EDLCs made with either type of electrolyte was very good (Figure 4c,d). A maximum operating frequency f_{max} (the frequency above which less than 50% capacitance is accessible) of up to ≈0.3 Hz is very high for ≈0.2 mm thick electrodes consisting of a strictly microporous carbon. In fact, it exceeds that of mesoporous carbon electrodes having a significantly larger pore volume[23] and indicates fast transport of ions.

As the operational temperature is lowered to –20 °C and –40 °C the superior performance of SBP-BF$_4$/AN:MF becomes apparent (**Figure 5**a,b). At these temperatures the standard electrolyte consistently shows a smaller capacitance for all the ZTC samples, which is particularly evident at faster slew rates. While the conductivity of the standard electrolyte is higher at these temperatures (Figure 3), its higher salt concentration and higher ion solvation energy likely limit its performance at temperatures below –20 °C. When the operational temperature is further dropped to –60 °C or below, the devices with a standard electrolyte cease to operate at meaningful levels (Figure 5c,d). Yet, the EDLCs based on ZTC electrodes and SBP-BF$_4$/AN:MF show outstanding performance. Due to the small pore size in ZTC, the electrode capacitances (up to 123 F g^{-1} or ≈76 F cm^{-3} at –60 °C and up to 117 F g^{-1} or ≈72 F cm^{-3} at –70 °C) and thus the energy storage characteristics of these EDLCs are higher than that of most commercial carbon electrodes operating at RT (commonly 75–85 F g^{-1} (≈25–45 F cm^{-3})[9k,14b,24]). The frequency response at –60 °C (f_{max} in excess of 0.1 Hz for ZTC

Materials
Views
www.MaterialsViews.com

ADVANCED
FUNCTIONAL
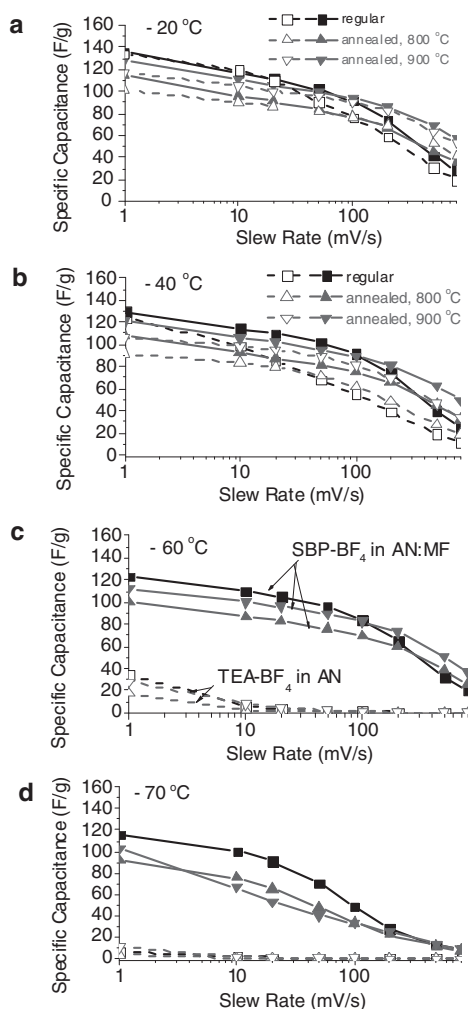MATERIALS
www.afm-journal.de

FULL PAPER

Figure 5. Specific capacitance of zeolite-templated carbons synthesized at 700 °C (regular and annealed for one hour at 800 and 900 °C) in conventional (TEA-BF$_4$ in AN; hollow symbols) and newly developed (SBP-BF$_4$ in AN:MF = 1:1; solid symbols) electrolytes calculated from the cyclic voltammetry (CV) curves of symmetric EDLCs as a function of sweep rate at a) –20 °C, b) –40 °C, c) –60 °C, and d) –70 °C.

Figure 6. Frequency response of capacitances of zeolite-templated carbons synthesized at 700 °C (regular and annealed for one hour at 800 and 900 °C) in conventional (TEA-BF$_4$ in AN; hollow symbols) and newly developed (SBP-BF$_4$ in AN:MF = 1:1; solid symbols) electrolytes at –60 °C.

Figure 7. Cyclic voltammograms of zeolite-templated carbons synthesized at 700 °C (regular and annealed for 1 hour at 800 and 900 °C) in conventional (TEA-BF$_4$ in AN; hollow symbols) and newly developed (SBP-BF$_4$ in AN:MF = 1:1; solid symbols) electrolytes at a slew rate of 1 mV s^{-1} recorded at –70 °C.

annealed at 900 °C, **Figure 6**) also exceeds that of commercial devices at RT (0.01–0.1 Hz[8a,24]), which indicates their superior power characteristics.

Figure 7 compares the shape of the cyclic voltammograms of EDLCs with the two studied electrolytes at –70 °C. In spite of the very low temperature, the EDLCs based on ZTC electrodes and SBP-BF$_4$/AN:MF electrolyte exhibit a nearly rectangular shape of the curve, indicative of nearly ideal EDLC behavior and unobstructed access of the electrolyte ions to most of the available surface area. Indeed, the supercapacitor electrodes at –70 °C retain 82–86% of their RT specific capacitance. In contrast, similar devices constructed with the standard TEA-BF$_4$/AN electrolyte (Figure 7) show a highly distorted curve and exhibit dramatically reduced energy and power storage capabilities. Thus, a careful design of the electrolyte is needed for the use of microporous carbon EDLCs at low temperatures.
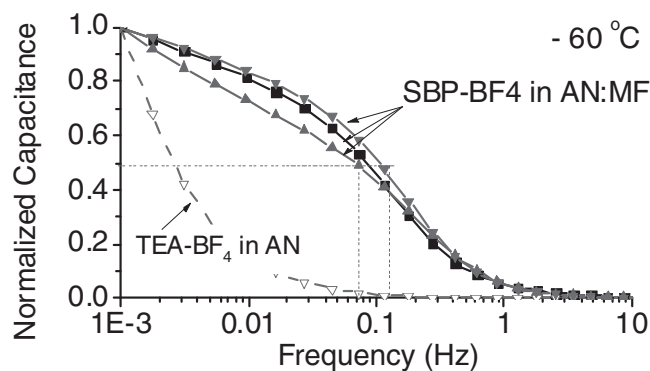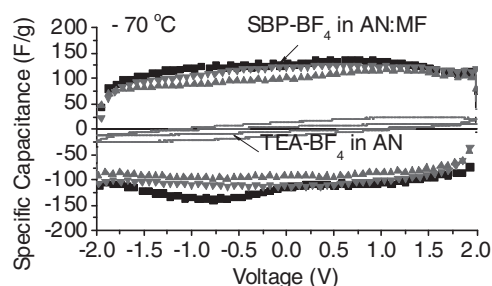
Figure 8 compares the low-temperature performance of mesoporous carbon (with an average mesopore size of ≈3 nm and a specific capacity of 65 F g^{-1} at room temperature) with that of ZTC in SBP-BF$_4$/AN:MF electrolyte. At temperatures as low as –60 °C (Figure 8a) and –70 °C (Figure 8b) ZTC show three times higher specific capacitance. In spite of having smaller pore size, ZTC show higher capacitance retention at faster sweep rate (Figure 8c) and better overall performance (Figure 8d). From these experiments we conclude that the enhanced low temperature performance of our EDLCs cannot be solely attributed to the novel electrolyte but necessitates a carbon that can efficiently facilitate the rapid electroadsorption of the salt ions onto its surface.

In order to reveal the effect of the salt dissolved in the same low temperature solvents, **Figure 9** compares the performance of TEA-BF$_4$ versus SBP-BF$_4$ in 1:1 AN:MF solution. As can be seen in the data, the positive impact of the SBP cations is evident at low temperatures. Both the value of the specific capacitance and the capacitance retention at –60 °C are noticeably better when using SBP-BF$_4$ as compared to the standard commercial TEA-BF$_4$ in the same solvent. This impact may stem from an increased energy of solvation for the TEA-BF$_4$ becoming more evident at lower temperatures as the thermal

**ADVANCED
FUNCTIONAL
MATERIALS**

www.afm-journal.de
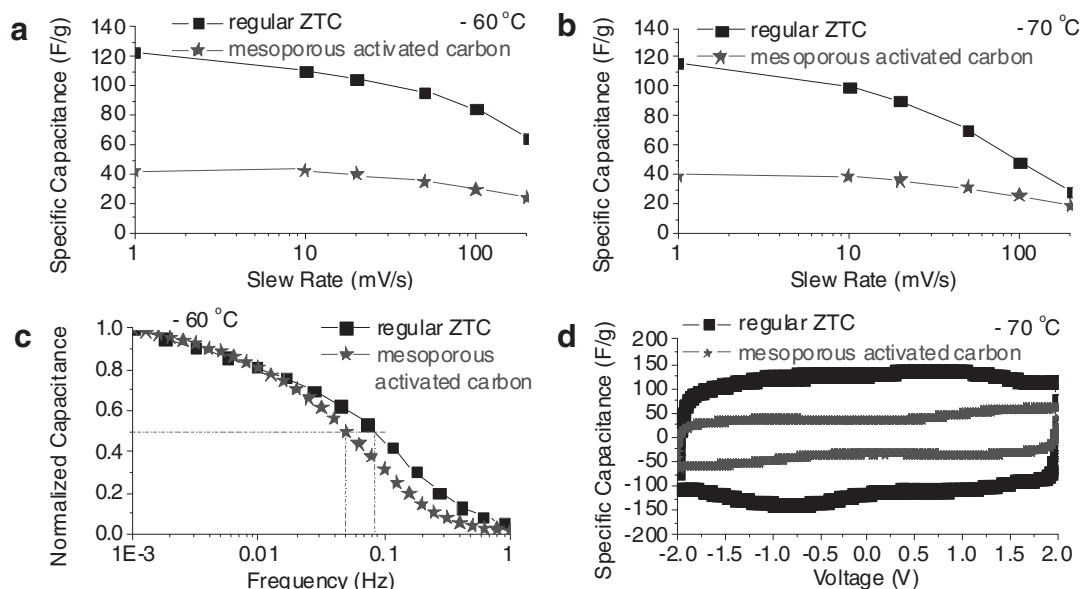
FULL PAPER

www.MaterialsViews.com

Figure 8. Comparison of the low-temperature performance of EDLCs based on ZTC and mesoporous activated carbons: specific capacitance calculated from the CV curves as a function of sweep rate at a) −60 °C and b) −70 °C. c) Frequency response of carbons and d) cyclic voltammograms at a slew rate of 1 mV s^{-1} recorded at −70 °C. Zeolite NaY-templated carbons synthesized at 700 °C and ARKEMA/CECA's Acticarbone activated carbon were used in the EDLC electrodes, while a solution of SBP-BF$_4$ in AN:MF = 1:1 solvent was used as electrolyte.

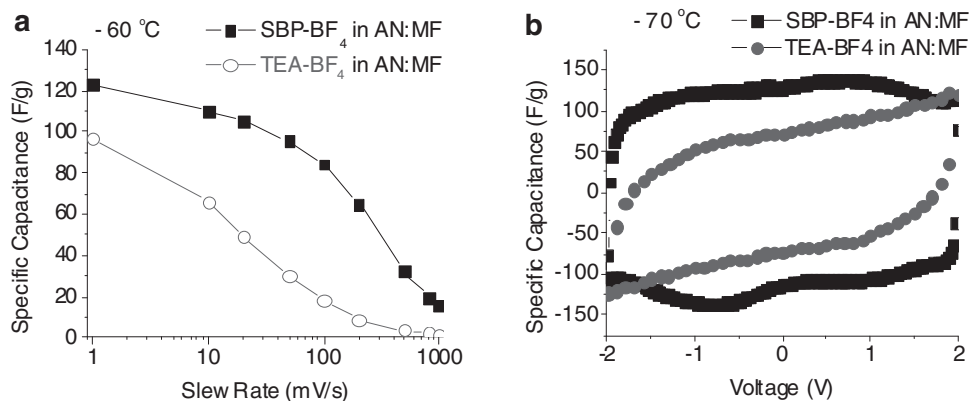**Figure 9.** Effect of the cation on the low-temperature performance of EDLCs utilizing AN:MF = 1:1 solvent: specific capacitance calculated from the CV curves as a function of sweep rate at a) −60 °C and b) cyclic voltammograms at a slew rate of 1 mV s^{-1} recorded at −70 °C. Zeolite NaY-templated carbons synthesized at 700 °C were used as electrodes and TEA-BF$_4$ and SBP-BF$_4$ salts were used in the electrolyte.

energy of the system is reduced. This increased energy barrier makes it more difficult to distort or remove the solvation shell and impedes the ability of the fully or partially solvated ions to efficiently organize into the most possibly compact layer. Improved ion mobility and resistance is further evinced by Figure 9b, which demonstrates the lower specific capacitance and increased ionic resistance for the TEA-BF$_4$ salt at −70 °C.

To the best of our knowledge, there are no other devices available that show stable performance and comparable electrochemical characteristics at −60 and −70 °C. Our findings address the need for high-power, rechargeable energy storage devices to operate at low temperatures in a growing number of important applications, where solid state capacitors cannot provide even remotely sufficient gravimetric and volumetric energy

density. Further systematic studies of the electrolyte properties (optimization of the salt and solvent composition for low temperature performance) combined with designing microporous carbons with straight pores and microstructure and pore size tuned for an optimum combination of high capacitance and rapid ion transport, which is electrolyte specific, will permit even higher power and energy characteristics and lower operating temperatures.

3. Conclusion

In summary, the low pressure decomposition of acetylene precursor onto a sacrificial zeolite template resulted in the

www.MaterialsViews.com

ADVANCED
FUNCTIONAL
MATERIALS
www.afm-journal.de

FULL PAPER

formation of uniform microporous carbons with high surface area and high energy and power performance characteristics when used in EDLCs with organic electrolytes. At room temperature the ≈0.2 mm thick electrodes produced with the synthesized microporous ZTC exhibited excellent ion transport and electroadsorption characteristics with capacitances in the range of 100–146 F g^{-1} (≈55–90 F cm^{-3}) and a maximum operating frequency of up to 0.3 Hz in organic electrolytes. Our studies further demonstrated that mesopores, which commonly reduce the specific and volumetric carbon capacitance, are not needed for high-power EDLC operation even at ultralow temperatures. The synergetic use of microporous ZTC and carefully designed electrolyte (SBP-BF$_4$ in 1:1 AN:MF) demonstrated an unprecedented combination of high volumetric and specific capacitance, rapid charging/discharging ability and high energy density characteristics at –70 °C (up to 86% of the energy density available at room temperature). These results open up many opportunities for high-energy electrochemical capacitor utilization for energy efficient applications in space vehicles, high-altitude aerial vehicles, polar regions and extreme altitudes, and facilitating the efficient utilization of renewable energy resources.

4. Experimental Section

Material Preparation: Zeolite NaY powder (product number: CBV100, Zeolyst International, Delfzijl, Netherlands) was placed in a 10 cm long quartz boat and heated inside a 3 cm in diameter horizontal quartz tube, which was placed in a Barnstead Thermolyne 21100 tube furnace, to the desired temperature under Ar flow at low pressures (<10 Torr). Once the desired temperature was reached, the Ar flow was halted and acetylene gas was then allowed to flow over the zeolite powder at a flow rate of 100 sccm at low pressures (<10 Torr) for the desired time. After deposition, the acetylene flow was stopped and the carbon-coated zeolite powder was allowed to cool to 200 °C before retrieval. Selected samples were post-annealed under the Ar flow prior to cooling down to 200 °C. After the carbon deposition, the carbon-coated zeolite powder was submerged in an HF solution (50%) for at least one day, after which the powder was washed with distilled water. The remaining impurities were removed via additional etching in H$_2$SO$_4$ (98%) for at least 1 day, followed by distilled water wash. Finally, the powder was washed in distilled water at 90 °C for 1 h and subsequently filtered. All porous carbon samples that were produced were then placed under vacuum to dry for at least 12 h.

The carbon powders were suspended in ethanol and mixed with polytetrafluoroethylene (PTFE) (60 wt% water suspension, Sigma Aldrich, USA) binder to form slurry consisting of carbon (95% wt) and PTFE (5% wt.). After drying overnight at 80 °C under vacuum the electrodes were calendared to a thickness of ≈0.2 mm using a commercial rolling mill and left to dry in a vacuum oven at 80 °C for 4–12 h prior to device assembling. The EDLCs were assembled in a symmetrical two-electrode configuration using 2016 stainless steel coin cells. Al foil was roughened using a 600 grit SiC sandpaper, coated by a thin layer (≈10 μm) of conductive paint (Superior Graphite), and used as a current collector. The conductive paint was used to reduce the interfacial resistance between the electrode and the current collector. A GORE membrane (W.L. Gore and Associates, US) of ≈25 μm in thickness and ≈60% porosity was used as the separator for the EDLC devices. Electrolytes were prepared in inert atmosphere gloveboxes, filled with Ar and containing less than 2 ppm of H$_2$O. For the preparation of the novel electrolyte, AN and MF (Sigma Aldrich, USA) were mixed in a 1:1 volume ratio, and SBP-BF$_4$ (0.25 M) (Japan Carlit Co., Ltd.) (except for the mesoporous activated carbon sample that employed 0.5 M SBP-BF$_4$ and the ZTC sample using TEA-BF$_4$ in AN:MF was 0.5 M) was dissolved in the blend with magnetic

stirring at room temperature. The sample containing TEA-BF$_4$ in AN:MF was at a 0.5 M concentration.

Testing: The cyclic voltammetry (CV) tests were carried out using a Solartron 1287 Electrochemical Interface in the voltage range between –2 and + 2 V. The gravimetric capacitance, C (F g^{-1}), was calculated according to:

$$C = \frac{2I}{(dV/dt)m} \qquad (1)$$

where I is the current (A), dV/dt is the slope of the discharge curve (V s^{-1}), and m is the average mass of the carbon electrode (g). Potentiostatic electrochemical impedance spectroscopy studies were carried out using a Zahner IM6 electrochemical workstation (Zahner-Elektrik, Germany) in the frequency range of 1 mHz to 100 kHz with a 10 mV AC amplitude. The specific capacitance was calculated according to:

$$C = \frac{2\,\left|\mathrm{Im}(Z)\right|}{2\pi f\left[(\mathrm{Im}(Z))^2 + (\mathrm{Re}(Z))^2\right]m} \qquad (2)$$

where f is the operating frequency (Hz), $\mathrm{Im}(Z)$ and $\mathrm{Re}(Z)$ are the imaginary and real parts of the total device impedance, and m is the mass of carbon in each electrode. The equation was expanded to allow for the mass magnitude to modify the contribution of each electrode.

The N$_2$ adsorption isotherms were measured at 77 K using a Micromeritics ASAP 2420 instrument. Ultrahigh purity N$_2$ gas (99.99%, Airgas, USA) was used for all experiments. Prior to the adsorption measurements the samples were outgassed for 12 h at 620 K under high vacuum. For the pore size distribution (PSD) analysis, the adsorption model isotherms (kernel) calculated using the nonlocal density functional theory (DFT) of Tarazona[25] implemented by Lastoskie et al. were applied.[26] In the DFT calculations parameters reported elsewhere were used.[27] To calculate PSDs of the carbons the numerical algorithm SAIEUS[28] that fits the kernel to the experimental data was used. BET SSA was calculated in the range of relative pressures from 0.05 to 0.15. SEM studies were performed using a LEO 1530 SEM microscope (LEO, Osaka, Japan, now Nano Technology Systems Division of Carl Zeiss SMT, MA, USA). An in-lens secondary electron detector was used for the studies, most of which were performed using an accelerating voltage of 5 kV and a working distance of 3 mm. TEM observations were carried out using a Philips CM200UT microscope that has 1.8 A point-to-point resolution and operates at 200 kV.

[1] a) K. N. Casper, *Nat. Resour. J.* **2010**, *49*, 825; b) N. Snow, *Oil Gas J.* **2010**, *108*, 26.

[2] J. S. Lawrence, M. C. B. Ashley, S. Hengst, D. M. Luong-Van, J. W. V. Storey, H. Yang, X. Zhou, Z. Zhu, *Rev. Sci. Instrum.* **2009**, *80*, 10.

[3] a) C. D. Thomas, A. Cameron, R. E. Green, M. Bakkenes, L. J. Beaumont, Y. C. Collingham, B. F. N. Erasmus, M. F. de Siqueira, A. Grainger, L. Hannah, L. Hughes, B. Huntley, A. S. van Jaarsveld, G. F. Midgley, L. Miles, M. A. Ortega-Huerta, A. T. Peterson, O. L. Phillips,

S. E. Williams, *Nature* **2004**, *427*, 145; b) M. Scheffer, S. Carpenter, J. A. Foley, C. Folke, B. Walker, *Nature* **2001**, *413*, 591.

[4] J. P. Matthews, A. J. Smith, I. D. Smith, *Planet Space Sci.* **1979**, *27*, 1391.

[5] a) J. S. Cloyd, *IEEE Aerosp. Electron. Syst. Mag.* **1998**, *13*, 17; b) J. A. Rosero, J. A. Ortega, E. Aldabas, L. Romeral, *IEEE Aerosp. Electron. Syst. Mag.* **2007**, *22*, 3.

[6] a) C. R. Sides, C. R. Martin, *Adv. Mater.* **2005**, *17*, 125; b) S. S. Zhang, K. Xu, T. R. Jow, *Electrochim. Acta* **2004**, *49*, 1057.

[7] a) P. Simon, Y. Gogotsi, *Nat. Mater.* **2008**, *7*, 845; b) J. R. Miller, P. Simon, *Science* **2008**, *321*, 651.

[8] a) W. C. West, M. C. Smart, E. J. Brandon, L. D. Whitcanack, G. A. Plett, *J. Electrochem. Soc.* **2008**, *155*, A716; b) E. J. Brandon, W. C. West, M. C. Smart, L. D. Whitcanack, G. A. Plett, *J. Power Sources* **2007**, *170*, 225.

[9] a) I. Kovalenko, D. Bucknall, G. Yushin, *Adv. Funct. Mater.* **2011**, *20*, 3979; b) J. Li, I. Zhitomirsky, *Colloid Surface A.* **2009**, *348*, 248; c) T. R. Jow, J. P. Zheng, *J. Electrochem. Soc.* **1998**, *145*, 49; d) C. Portet, Z. Yang, Y. Korenblit, Y. Gogotsi, R. Mokaya, G. Yushin, *J. Electrochem. Soc.* **2009**, *156*, A1; e) C. Portet, G. Yushin, Y. Gogotsi, *Carbon* **2007**, *45*, 2511; f) C. O. Ania, V. Khomenko, E. Raymundo-Pinero, J. B. Parra, F. Beguin, *Adv. Funct. Mater.* **2007**, *17*, 1828; g) D. Hulicova-Jurcakova, M. Seredych, G. Q. Lu, T. J. Bandosz, *Adv. Funct. Mater.* **2009**, *19*, 438; h) D. Hulicova-Jurcakova, M. Kodama, S. Shiraishi, H. Hatori, Z. H. Zhu, G. Q. Lu, *Adv. Funct. Mater.* **2009**, *19*, 1800; i) L. Wei, M. Sevilla, A. B. Fuertesc, R. Mokaya, G. Yushin, *Adv. Energy Mater.* **2011**, *1*, 356; j) M. Rose, Y. Korenblit, E. Kockrick, L. Borchardt, M. Oschatz, S. Kaskel, G. Yushin, *Small* **2011**; k) Y. Korenblit, M. Rose, E. Kockrick, L. Borchardt, A. Kvit, S. Kaskel, G. Yushin, *ACS Nano* **2010**, *4*, 1337; l) A. Kajdos, A. Kvit, F. Jones, J. Jagiello, G. Yushin, *J. Am. Chem. Soc.* **2010**, *132*, 3252; m) L. Wei, M. Sevilla, A. B. Fuertesc, R. Mokaya, G. Yushin, *Adv. Funct. Mater.* DOI: 10.1002/adfm.201101866.

[10] B. E. Conway, *Electrochemical Supercapacitors*, Vol. 1, Kluwer Academic/Plenum Publishers, New York, **1999**.

[11] a) A. Kajdos, A. Kvit, F. Jones, J. Jagiello, G. Yushin, *J. Am. Chem. Soc.* **2010**, *132*, 3252; b) M. Rose, Y. Korenblit, E. Kockrick, L. Borchardt, M. Oschatz, S. Kaskel, G. Yushin, *Small* **2011**; c) C. G. Liu, Z. N. Yu, D. Neff, A. Zhamu, B. Z. Jang, *Nano Lett.* **2010**, *10*, 4863.

[12] C. Portet, G. Yushin, Y. Gogotsi, *J. Electrochem. Soc* **2008**, *155*, A531.

[13] a) D. Pech, M. Brunet, H. Durou, P. H. Huang, V. Mochalin, Y. Gogotsi, P. L. Taberna, P. Simon, *Nat. Nanotechnol.* **2010**, *5*, 651; b) J. R. Miller, R. A. Outlaw, B. C. Holloway, *Science* **2010**, *329*, 1637; c) C. S. Du, J. Yeh, N. Pan, *Nanotechnology* **2005**, *16*, 350.

[14] a) C. Portet, P. L. Taberna, P. Simon, E. Flahaut, C. Laberty-Robert, *Electrochim. Acta* **2005**, *50*, 4174; b) J. Gamby, P. L. Taberna, P. Simon, J. F. Fauvarque, M. Chesneau, *J. Power Sources* **2001**, *101*, 109.

[15] a) J. Chmiola, G. Yushin, Y. Gogotsi, C. Portet, P. Simon, *Science* **2006**, *313*, 1760; b) E. Raymundo-Pinero, K. Kierzek, J. Machnikowski, F. Beguin, *Carbon* **2006**, *44*, 2498; c) J. S. Huang, B. G. Sumpter, V. Meunier, *Angew. Chem. Int. Ed.* **2008**, *47*, 520; d) J. S. Huang, B. G. Sumpter, V. Meunier, *Chem.-Eur. J.* **2008**, *14*, 6614.

[16] a) J. Chmiola, G. Yushin, R. K. Dash, E. N. Hoffman, J. E. Fischer, M. W. Barsoum, Y. Gogotsi, *Electrochem. Solid St.* **2005**, *8* A357; b) E. N. Hoffman, G. Yushin, T. El-Raghy, Y. Gogotsi, M. W. Barsoum, *Microporous Mesoporous Mater.* **2008**, *112*, 526; c) G. Yushin, R. K. Dash, Y. Gogotsi, J. Jagiello, J. E. Fischer, *Adv. Funct. Mater.* **2006**, *16*, 2288; d) C. Portet, G. Yushin, Y. Gogotsi, *J. Electrochem. Soc* **2008**, *155*, A531.

[17] T. Kyotani, Z. X. Ma, A. Tomita, *Carbon* **2003**, *41*, 1451.

[18] K. Chiba, T. Ueda, H. Yamamoto, *Electrochemistry* **2007**, *75*, 664.

[19] R. T. Yang, *Adsorbents: Fundamentals and Applications*, Wiley & Sons, Inc., Hoboken, NJ, **2003**.

[20] S. W. Lee, N. Yabuuchi, B. M. Gallant, S. Chen, B.-S. Kim, P. T. Hammond, Y. Shao-Horn, *Nat. Nanotechnol.* **2010**, *5*, 531.

[21] G. Feng, R. Qiao, J. S. Huang, B. G. Sumpter, V. Meunier, *ACS Nano* **2010**, *4*, 2382.

[22] J. S. Huang, B. G. Sumpter, V. Meunier, G. Yushin, C. Portet, Y. Gogotsi, *J. Mater. Res.* **2010**, *25*, 1525.

[23] D. W. Wang, F. Li, M. Liu, G. Q. Lu, H. M. Cheng, *Angew. Chem. Int. Ed.* **2008**, *47*, 373.

[24] P. L. Taberna, P. Simon, J. F. Fauvarque, *J. Electrochem. Soc.* **2003**, *150*, A292.

[25] P. Tarazona, *Phys. Rev. A.* **1985**, *31*, 2672.

[26] C. Lastoskie, K. E. Gubbins, N. Quirke, *J. Phys. Chem* **1993**, *97*, 4786.

[27] P. I. Ravikovitch, A. Vishnyakov, R. Russo, A. V. Neimark, *Langmuir* **2000**, *16*, 2311.

[28] J. Jagiello, *Langmuir* **1994**, *10*, 2778.